Relaxor ground state forced by ferroelastic instability in $K_{0.5}Bi_{0.5}TiO_3$-$Na_{0.5}Bi_{0.5}TiO_3$

Gobinda Das Adhikary,[1] Bhoopesh Mahale,[1] Anatoliy Senyshyn,[2] and Rajeev Ranjan[1,*]

[1]*Department of Materials Engineering, Indian Institute of Science, Bangalore-560012, India*

[2]*Forschungsneutronenquelle Heinz Maier-Leibnitz (FRM II), Technische Universität München, Lichtenbergestrasse 1, D-85747 Garching b. München, Germany*

(Received 29 September 2020; revised 5 November 2020; accepted 10 November 2020; published 23 November 2020)

The complex interplay of local disorder with the structure and dynamics and their role in enhancing the electromechanical response makes relaxor ferroelectric materials fascinating both from the scientific and technological standpoints. It is generally believed that in chemically disordered ferroelectric solid solutions, the normal ferroelectric state gradually yields to a relaxor ground state on increasing the concentration of localized (point-defect-like) random-field centers. That a different kind of process can spontaneously stabilize a relaxor ground state is less known, especially in the family of ferroelectric perovskites. We demonstrate the occurrence of this less-known phenomenon in $(1-x)K_{0.5}Bi_{0.5}TiO_3$-$(x)Na_{0.5}Bi_{0.5}TiO_3$[$(1-x)$KBT − (x)NBT]. Unlike the gradual evolution common to most ferroelectric solid solutions, KBT-xNBT exhibits an abrupt crossover from a normal ferroelectric ground state to a full-blown relaxor ground state for $x > 0.58$. We show that this abrupt crossover to the relaxor state is caused by stabilization of an incommensurate-like/highly disordered M-point ferroelastic distortion in the ergodic/paraelectric temperature regime. The abrupt crossover manifests as composition driven anomalous changes in several important properties such as dielectric response, electromechanical properties, tetragonality, and coercive field, electrostrain, and mimics a scenario often encountered in composition driven interferroelectric transformations.

DOI: 10.1103/PhysRevB.102.184113

I. INTRODUCTION

Perovskite-based relaxor ferroelectric materials are interesting both from the scientific and technological standpoints. Apart from offering model systems for understanding the underlying physics governing the complex evolution of polarization amid structural disorder in crystals, such materials show giant electromechanical response [1–4] and are highly sought after as high-performance actuators and transducers devices. In contrast to normal ferroelectrics, which exhibit long-range polar order below the symmetry breaking Curie point (T_C), relaxor ferroelectrics exhibit polar nano regions (PNRs) and do not exhibit symmetry breaking on the global scale below the dielectric maximum temperature. The dynamic PNRs above the dielectric maximum temperature (T_m) gradually freeze on cooling below T_m and stabilizes a nonergodic relaxor ground state. There are differing viewpoints regarding the role of the PNRs in enhancing electromechanical response in ferroelectric systems [1,3,4,5–8]. From a phenomenological thermodynamic perspective, the local structural heterogeneities associated with PNRs contributes to the flattening of the free energy landscape making polarization rotation easier and increase the piezoelectric response [7]. A related viewpoint attributes the giant electromechanical response in ferroelectric relaxors to the occurrence of critical points that define a line in the electric-field–temperature–composition phase diagram [9]. Atomistic models, on the other hand, attribute the large electromechanical response to a phase instability induced by the PNR– transverse acoustic phonon interaction [10], and/or competing ferroelectric and antiferroelectric interactions [11–13].

It is believed that PNRs arise because of the breaking of the translational invariance by local random electric and/or strain fields. The randomness is associated with two or more cationic species occupying randomly the same crystallographic site. As such, chemical disorder in ferroelectric solid solutions/compounds with two or more cationic species is a necessary condition for driving a ferroelectric to a relaxor state. In stoichiometric compounds like $Pb(Mg_{1/3}Nb_{2/3})O_3$, the random field is also contributed by local 1:1 ordering of Mg^{+2} and Nb^{+5} ions causing lack of charge neutrality on the mesoscale [14–16]. That chemical disorder is important for the relaxor state has been proven by the fact that chemical ordering of Sc and Nb (by prolonged thermal annealing) in $Pb(Sc_{1/2}Nb_{1/2})O_3$ stabilizes the normal ferroelectric state [17,18]. However, in most multication ferroelectric systems chemical order is not practically feasible and makes relaxor ferroelectricity a common occurrence in ferroelectric solid solutions.

It may, however, be noted that chemical disorder in ferroelectric solid solutions does not necessarily guarantee a relaxor ferroelectric state such as in the classical piezoelectric system Pb(Zr, Ti)O_3 [19] and $PbTiO_3$-$BiScO_3$ [20–22]. Both these systems exhibit normal ferroelectric behavior in their respective solid solubility range and show morphotropic phase boundaries at which the piezoelectric properties are considerably enhanced [21,22]. Though

*rajeev@iisc.ac.in

competing ferroelectric-antiferroelectric instability [11–13] and/or incommensurate modulations [23,24] are plausible viewpoints to explain the loss of long-range polar order in relaxor ferroelectrics, the corresponding signatures are not often seen on the global scale making such a correlation difficult to establish experimentally. An intimate correlation between incommensurate (commensurate) structural modulation and relaxor (normal) ferroelectric behavior, on the other hand, has been demonstrated in the family of rare-earth tetragonal tungsten bronze (TTB) structures with chemical formula $Ba_4RE_2Ti_4Nb_6O_{30}$ (RE = rare earth) [25–29]. TTB compounds with radius of RE ions greater than 1.3 Å exhibit incommensurate distortion and relaxor behavior, whereas those with RE radius less than 1.3 Å show a commensurate phase and normal ferroelectric behavior. Zhu *et al.* [30] have reconfirmed the relative importance of the incommensurate/commensurate structural distortions vis-à-vis the relaxor/ferroelectric behavior and explained the incommensurate/commensurate distortions in terms of crystal-chemical concepts, such as positional disorder, ionic radius, polarizability, and point defects.

In this paper we show that an analogous situation, like in the TTB family of ferroelectric oxides, occurs in the perovskite-based ferroelectric solid solution $K_{0.5}Bi_{0.5}TiO_3$-$Na_{0.5}Bi_{0.5}TiO_3$ (KBT-NBT). Similar to $BaTiO_3$ (BT) and $PbTiO_3$ the average structure of KBT is tetragonal ($P4mm$). However, KBT exhibits a considerable structural disorder [31–35] due to random occupation of two different cations K and Bi on the A site. Despite the disorder, KBT behaves like a normal ferroelectric [36–38]. NBT too shows structural disorder and exhibits rhombohedral/monoclinic average structure [39,40] on the global scale. NBT and KBT exhibit complete solid solubility and show a morphotropic phase boundary (MPB) at $\sim$ 20 mole % KBT [35,41–44] at which the dielectric and piezoelectric properties are enhanced. Most studies on KBT-NBT (and its analog NBT-BT) in the past have focused on compositions close to the MPB. In this paper we show that the dielectric, ferroelectric, and electromechanical properties show another anomalous change in a narrow composition interval $0.58 < x < 0.60$ (in the tetragonal phase regime), far away from the MPB of $(1-x)$KBT-xNBT. However, unlike the interferroelectric instability that characterizes MPB, we show that the abrupt change in the polar properties for $x > 0.58$ is caused by system suddenly changing its ground state from a normal ferroelectric to a full blown relaxor state. Detailed investigation revealed that this abrupt crossover to the relaxor state is caused by the system stabilizing highly disordered M-point/incommensuratelike ferroelastic distortion in the paraelectric/ergodic temperature regime for $x > 0.58$.

II. EXPERIMENTAL DETAILS

Ceramic specimens of $(1-x)K_{0.5}Bi_{0.5}TiO_3$-$(x)Na_{0.5}Bi_{0.5}TiO_3$[$(1-x)$KBT-$x$NBT] were synthesized by a conventional solid solution route. Dried raw powders of TiO_2 (99.8%, Alfa Aesar), K_2CO_3 (99%, Alfa Aesar), Bi_2O_3 (99%, Alfa Aesar), Na_2CO_3 (99.5%, Alfa Aesar) were weighted according to stoichiometric proportions. The powders were thoroughly mixed in an ethanol medium using zirconia balls and vials in a planetary ball mill with a speed of 150 rotations per minutes for 12 h. The mixed powder was calcined at 900 °C for 3 h in covered alumina crucibles. The calcined powders were milled again at 150 rpm for 8 h. 5% polyvinyl alcohol was added to the dried remilled powders and then compressed into pellets under uniaxial pressure of 100 MPa completed by cold isotropic pressure of (250–300 MPa). The green pellets were sintered in a muffle furnace at 1065–1150 °C for 4 h by placing them on a platinum sheet and covered by alumina crucibles. A sacrificial powder of similar composition was used to compensate for the evaporation of volatile elements. The sintered pellets show average density $\sim$ 95% (with respect to the theoretical density). For electrical measurements, both the surfaces of the sintered pellets (diameters of 10–12 mm and thickness of 0.3 mm) were painted with high temperature silver paste and subsequently fired at 550 °C. Electrical poling was performed for 30 min at a field of 60 kV/cm dc field. Direct piezoelectric coefficient (d_{33}) of poled pellet was measured using Piezotest, PM300 with applied force 0.25 N and frequency 110 Hz. A Precision Premier II tester (Radiant Technologies, Inc.) was used to obtain the polarization–electric field hysteresis and electrostrain-electric field measurements. Raman spectra were collected from poled and unpoled pellets using 532 nm laser attached with LabRAM HR (HORBA) spectrometer. The dielectric measurements were carried out using a Novocontrol Alpha-A impedance analyzer. Neutron powder diffraction data were collected at the diffractometer SPODI at FRM-II, Germany (wavelength of 1.548150 Å) [45]. X-ray powder diffraction (XRPD) was carried out using a Rigaku Smartlab x-ray diffractometer with monochromatic Cu $K\alpha_1$ radiation. XRPD of the poled specimens were obtained after crushing the poled pellets gently to powder. The XRPD patterns of the unpoled specimens were collected after annealing the powder at 700 °C for 2 h obtained after crushing the sintered pellets to remove the effect of residual stress incurred during the grinding process. Structural analysis was performed by the Rietveld method using the FULLPROF software [46].

III. RESULTS

A. Anomalous change in physical properties

Figure 1(a) shows the composition (x) dependence of the weak-field longitudinal piezoelectric coefficient (d_{33}) of $(1-x)$KBT–(x)NBT. The piezoelectric response (d_{33}) increases very sharply from 130 pC/N at $x = 0.58$ to to 167 pC/N at $x = 0.60$. The composition dependence of relative permittivity of the unpoled specimens also shows a sharp increase at $x = 0.60$ [Fig. 1(b)]. Though the permittivity is reduced after poling, the abrupt change in the permittivity can still be seen at $x = 0.60$. Concomitantly, there is abrupt drop in the coercive field (E_c), Fig. 1(c). The remnant polarization shows a peak around the same value, Fig. 1(d). Electrostrain measurements reveal a sharp increase in the bipolar strain from 0.10% for $x = 0.58$ to 0.25% for $x = 0.60$ (measured with field amplitude 55 kV/cm.) The corresponding unipolar electrostrain increased remarkably from 0.08% for $x = 0.58$ to 0.20% for $x = 0.60$, Fig. 1(e). We also determined the depolarization temperature from the peak in the temperature dependent of the pyro-current of poled

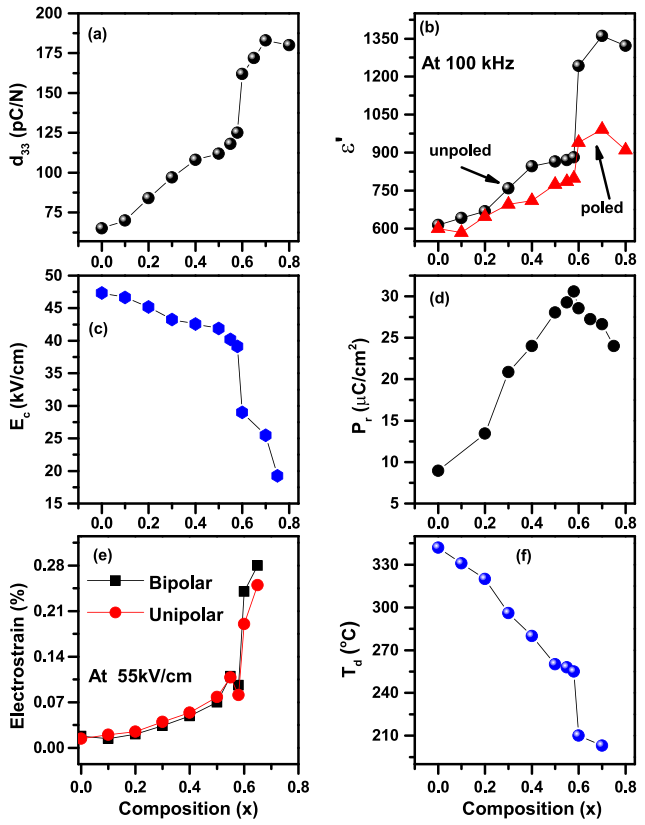

FIG. 1. Composition dependence of (a) longitudinal piezoelectric coefficient (d_{33}) and (b) dielectric constant (ε') of both unpoled and poled $(1-x)$KBT $-$ xNBT specimens. (c) and (d) shows the composition dependence of the coercive field and remnant polarization, respectively. The composition dependence of the unipolar and bipolar electrostrain measured at 55 kV/cm (at 1 Hz) is shown in (e). (f) shows the composition dependence of depolarization temperature (T_d).

specimens, Fig. S1 in the Supplemental Material [47]. Although the anomalous change in the properties across the narrow composition interval $0.58 < x < 0.60$ mimics a situation equivalent to a composition driven interferroelectric transformation, the abrupt decrease in the depolarization temperature for $x > 0.58$ [Fig. 1(f)] is not consistent with a composition driven interferroelectric instability in most ferroelectric solid solutions [48]. In a conventional ferroelectric such as $Pb(Zr, Ti)O_3$, $(Ba, Ca)(Zr, Ti)O_3$(BZT-xBCT), the Curie temperature, which is considered as depolarization temperature, varies monotonically with composition across the MPB, which exhibits a composition driven interferroelectric instability [48].

B. Abrupt ferroelectric-relaxor crossover

Figure 2(a) shows the temperature dependence of real part of relative permittivity for different compositions. Consistent with the previous studies [36–38,49], KBT ($x = 0.00$) exhibits a broad dielectric peak at $T_m \sim 380\,^{\circ}$C. The hump at a lower temperature 319 °C is attributed to a spontaneous temperature driven ferroelectric-relaxor transition (T_{F-R}) [36–38,49]. The sharp shoulder in the temperature permittivity plots persists until $x = 0.58$. For $x > 0.58$ it disappears and is replaced by another broad dielectric maximum [Fig. 2(a) and Supplemental Material [47] Fig. S2]. This is more clearly manifested in the imaginary part of the permittivity [Fig. 2(b). The frequency dispersion in the dielectric maximum temperature of the imaginary part suggests that the broad anomaly at low temperature is associated with relaxor behavior [Figs. S3 and S4, Supplemental Material [47]). The system has abruptly changed its ground state from a normal ferroelectric for $x \leqslant 0.58$ to a relaxor state for $x > 0.58$. We also found abrupt change in the high temperature properties like the temperature of maximum relative permittivity (T_m), the Curie-Weiss temperature (T_{CW}), and the Burn's temperature (T_B), Fig. S5. This suggests that the abrupt transition to the relaxor behavior is also related to a qualitative change in the property of the lattice in the ergodic/paraelectric state for $x > 0.58$.

C. Increased structural disorder for $x > 0.58$: XRD study

The XRPD pattern of the unpoled specimens of $(1-x)$KBT-(x)NBT suggest tetragonal ($P4mm$) structure for $x \leqslant 0.58$ in Fig. S6. For $0.58 < x < 0.75$ the XRPD patterns could be fitted satisfactorily by considering the coexistence of cubic and tetragonal structural model (Fig. S7, Supplemental Material [47]). It is interesting to note a one-to-one correlation between the abrupt decrease in the tetragonality of the tetragonal phase and the onset of the cubiclike phase [Figs. 2(c) and S7]. The cubic peaks are not clearly visible, and the structure appears tetragonal ($P4mm$) for all the poled compositions investigated here [Fig. 2(d)]. We may note that the XRPD patterns of poled specimens were collected on ground powder of poled pellets. This strategy allows us to get a preferred orientation free diffraction pattern while the individual grains retains the irreversible structural changes brought about by the poling field [50,51]. The disappearance of the cubic peaks in the diffraction patterns of poled specimen suggests that the cubiclike phase seen in the unpoled $x > 0.58$ are volume averaged short ranged tetragonal regions. A similar cubiclike phase has been reported in other NBT-based piezoelectrics and is attributed to short-range correlations of polar distortion [52,53]. In our case, poling increases the correlation length of the short-range tetragonal regions. This manifests as poling induced cubic to tetragonal transformation on the global scale [3,4,54]. Interestingly, the tetragonality (c/a) of the poled specimens too exhibits an abrupt decrease for $x > 0.58$. In view of the correlation between disorder and tetragonality observed for the unpoled specimens [Fig. 2(c)], we suspected a similar correlation in the poled specimens. This was proved by Rietveld analysis (Fig. S8), which reveals an abrupt increase in the volume fraction of the disordered regions (cubic phase) for $x > 0.58$, Fig. 2(e).

D. Anomalous structural changes for $x > 0.58$: Raman study

Raman spectroscopy is a powerful tool to probe structural features on a short length scale [55]. Figure 3(a) depicts the Raman spectra after Bose-Einstein correction for various compositions of (x)NBT-$(1-x)$KBT in the unpoled state. The Raman spectra of pure KBT is identical to what has been

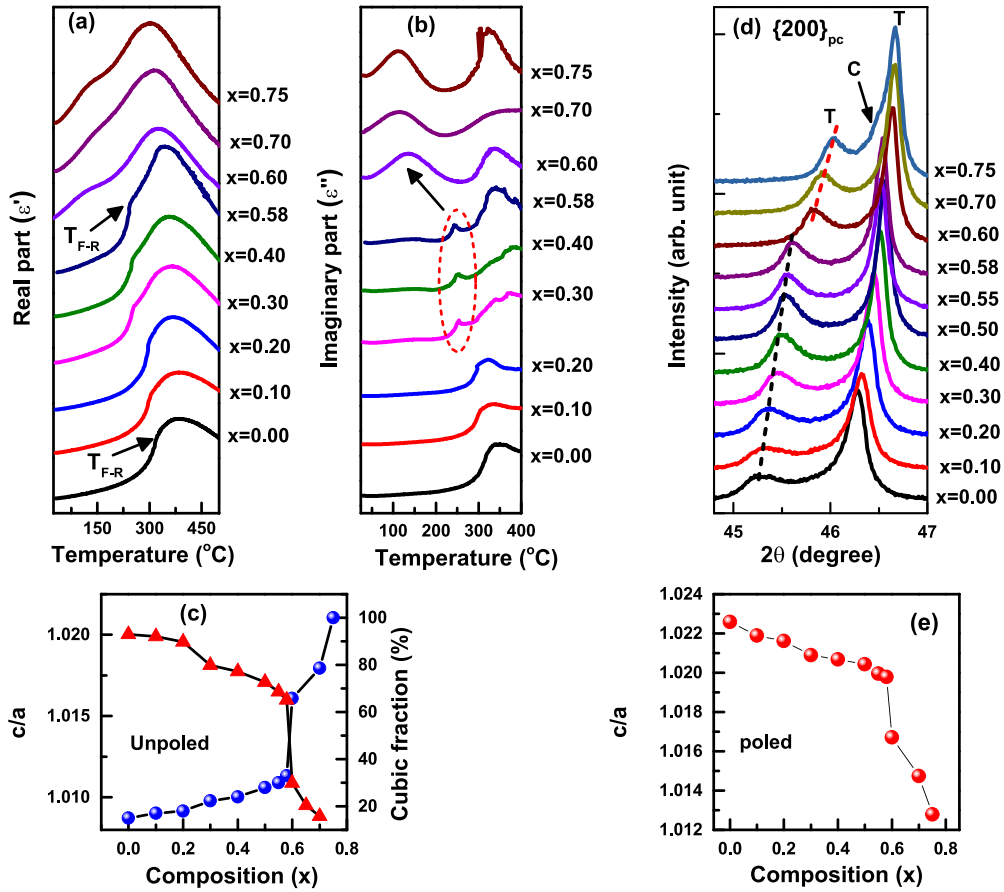

FIG. 2. (a) Real part of dielectric permittivity as a function of temperature measured at 10 kHz for several compositions of $(1-x)$KBT $-$ (x)NBT system. T_{F-R} indicates ferroelectric to relaxor transition temperature. (b) Temperature dependence of imaginary part of dielectric permittivity at the same frequency. (c) composition dependence of tetragonality (c/a) and cubic phase fractions for unpoled $(1-x)$KBT $-$ (x)NBT specimens. (d) Evolution of $\{200\}_{pc}$ Bragg profile of poled compositions. T and C represent tetragonal ($P4mm$) phase and cubic ($Pm-3m$) phase, respectively. (e) Tetragonality (c/a) of poled specimens as a function of composition.

reported earlier by Kreisel *et al.* [56]. The spectrum are mainly centered in three wave-number regions. We assign them as A band ($100-200\,\mathrm{cm}^{-1}$), B band ($200-400\,\mathrm{cm}^{-1}$), and C band ($400-650\,\mathrm{cm}^{-1}$). The mode in A band is associated with the Na/K-O vibration, in the B band with Ti-O vibration, and in the C band with vibrations involving oxygen displacements [56,57]. For convenience of labeling and following earlier reports [58], the peak in the range $\sim 109-116\,\mathrm{cm}^{-1}$ ($\omega_1-\omega_2$) is labeled as E(TO1) and $130-150\,\mathrm{cm}^{-1}$ (ω_3) by A_1(TO1) mode. The other peaks are assigned as E (TO2) $\sim 215\,\mathrm{cm}^{-1}$ (ω_4), A_1 (TO2) $\sim 280\,\mathrm{cm}^{-1}$ (ω_5), [E(LO2) + B1] $\sim 350\,\mathrm{cm}^{-1}$ (ω_6), E (LO3) $\sim 510\,\mathrm{cm}^{-1}$ (ω_7), E (TO3) $\sim 540\,\mathrm{cm}^{-1}$ (ω_8), and A_1(TO3) $\sim 630\,\mathrm{cm}^{-1}$ (ω_9). Quantitative analysis of the Raman data was carried out by fitting the spectrum with Lorentzian functions, Figs. 3(b) and S9 in the Supplemental Material [47]. Some of the changes that can be identified visibly across the narrow composition interval $0.58 < x < 0.60$ are (i) disappearance of the E(TO2) mode at $\sim 215\,\mathrm{cm}^{-1}$; (ii) merger of the split bands centered around $315\,\mathrm{cm}^{-1}$ at $x = 0.60$. We noted that the frequencies of the three modes ω_4, ω_5, ω_6 corresponding to the Ti-O vibration drops at $x = 0.60$, Fig. 3(c). The integrated intensities of these modes also exhibit anomalous change around this composition, Fig. S10, Supplemental Material [47]. The most notable change is the abrupt increase in the intensity of the mode at $\sim 115\,\mathrm{cm}^{-1}$ in Fig. 3(a). A similar enhancement in the intensity of this mode can be noted in the $P4bm$ phase of NBT at 310 °C, and for the MPB composition ($x = 0.06$) of the NBT-xBT series, Fig. S11, Supplemental Material [47]. This similarity seems to suggest the possibility of stabilizing in-phase octahedral for $x > 0.58$ in KBT-NBT.

E. The origin of structural-polar disorder: Neutron powder diffraction study

While both XRPD and Raman studies indicate onset of some kind of structural distortion which causes abrupt increase in the structural-polar disorder for $x > 0.58$ favoring the relaxor ground state (Fig. S12a, Supplemental Material [47]), it failed to reveal the nature of the distortion itself. We performed neutron powder diffraction (NPD) study of these specimens to get better insight regarding the possible origin of the structural-polar disorder. In contrast to XRPD, neutron diffraction can offer structural information associated with oxygen octahedral tilt due to comparable scattering amplitude of oxygen and the heavy cations. Figure 4 shows a vertically magnified NPD patterns of $(1-x)$KBT-(x)NBT in a limited 2θ range. For $x \leqslant 0.58$, the diffraction pattern can be

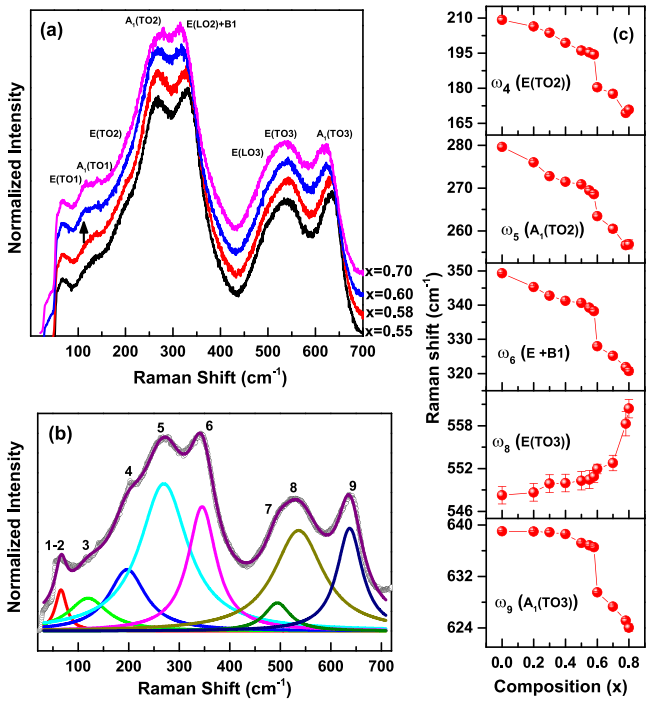

FIG. 3. (a) Room temperature Raman spectra for $(1-x)$KBT $-$ xNBT. The arrow shows the abrupt increase in the intensity of the mode at $\sim$115 cm^{-1}. (b) Raman spectrum of $x = 0.00$ fitted with Lorentzian profiles. (c) Raman shift (cm^{-1}) in the Raman spectra of $(1-x)$KBT $-$ xNBT as a function of composition.

explained with the tetragonal ($P4mm$) structural model, Figs. S13a, 13b, Supplemental Material [47]. For $x \geqslant 0.60$, weak superlattice reflections become noticeable in the NPD patterns. Evidently, the tetragonal $P4mm$ model cannot account for these superlattice reflection (Fig. S14a). These superlattice

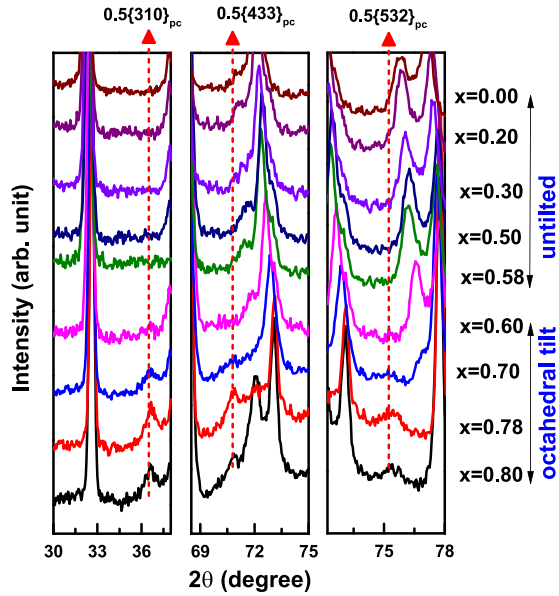

FIG. 4. Part of the neutron powder diffraction pattern of $(1-x)$KBT $-$ (x)NBT. The arrows indicate superlattice reflections. The indices are labeled with respect to the pseudocubic cell.

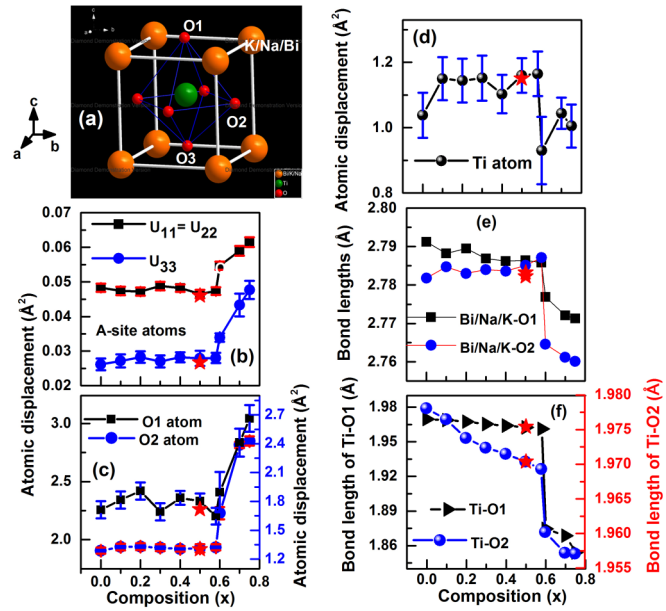

FIG. 5. (a) Unit cell of tetragonal structure for the composition $x = 0.50$. Atomic displacement of (b) A-site atoms, (c) O1 and O2 atoms, (d) Ti atoms as a function of compositions. (e) Bond lengths of Bi/Na/K-O1, Bi/Na/K-O2, and Bi/Na/K-O3 bonds as a function of composition. The number of each bond is 4. (f) Bond lengths of long Ti-O1 bond (no of bond-1) and short Ti-O2 bond (no of bonds-1) as a function of composition. Note: These structural parameters were calculated after fitting the room temperature NPD pattern of unpoled $x \leqslant 0.58$ composition and the NPD pattern of poled $0.75 \geqslant x \geqslant 0.60$ compositions with $P4mm$ structural model. The data points shown by red star are for poled $x = 0.50$ composition.

reflections cannot be accounted for by the prevalent $P4bm$ tetragonal structural model (See Fig. S14b, Supplemental Material [47]), which is generally invoked to explain in-phase octahedral tilt in NBT-based systems. In fact, it was not even possible to index them using a $2 \times 2 \times 2$ supercell of the basic $P4mm$ unit cell (Fig. S14c, Supplemental Material [47]). A possible explanation could be that the in-phase octahedral distortion is highly disordered and the inability to account for the superlattice peaks in the NPD is due to superposition of the complex three-dimensional diffuse scattering signal onto one dimension. Alternatively, it may correspond to an incommensurate/long-period modulation of the octahedral tilt configuration [44,59–61].

Although we could not account for the superlattice reflections, for the sake of a comparative understanding of the evolution of the structural parameters, we persisted with fitting the NPD patterns using $P4mm$ structural model (Fig. S13) for all compositions in the tetragonal regime. Since the XRPD of poled $x > 0.58$ show only tetragonal peaks, for the sake of consistency and meaningful comparison with the refined tetragonal ($P4mm$) structural parameters of $x \leqslant 0.58$, we carried out Rietveld analysis of $x > 0.58$ using NPD pattern of poled specimens (Figs. 5, S13c, S13d). It is important to note that although the superlattice peaks (which persist in the poled specimen, though with a slightly reduced intensity) cannot be accounted for with the $P4mm$ model (Fig. S14d), the main Bragg profiles fit satisfactorily for the compositions

$x = 0.60$ and 0.70 (Figs. S13c, S13d). During the refinement we noted that the isotropic displacement parameters of the A-site cations (Na/K/Bi) was very high ($>4\,A^2$). For these cations, we refined the anisotropic displacement parameters. For the rest, we refined the isotropic displacement parameters to minimize the number of independent refinable parameters. The fact that the structural parameters of unpoled and poled $x = 0.50$ show almost identical values [Figs. 5(b)–5(f)] validates our strategy. The abrupt increase in the displacement parameters of both Na/K/Bi and O for $x > 0.58$ [Figs. 5(b)–5(d)] correlates perfectly well the onset of the octahedral tilt. Concomitantly, the A-O and the Ti-O bond distances shows an abrupt decrease for $x > 0.58$, Figs. 5(e) and 5(f). Both the features are consistent with the sudden decrease in the tetragonality of for $x > 0.58$, Fig. 2(c).

IV. DISCUSSION

Chemical substitutions in ferroelectric systems necessarily introduce a random field by virtue of either ionic size difference and/or local charge imbalance. In solid solutions exhibiting morphotropic phase boundaries, chemical substitutions primarily drive a structural-polar instability. In situations wherein MPB is not possible, the primary role of chemical substitution in a ferroelectric solid solution is to create random field centers that increasingly break the long-range ferroelectric order and eventually impart relaxor character to the system. In all these cases, the source of the disorder is randomly located point defects. In the phenomenological framework, Wang *et al.* have argued that the local polarization associated with such defect dipoles breaks the symmetry of the Landau free energy by introducing local minima [62]. At low concentration of such defects, the resistance to the development of a long-range ferroelectric correlation is not strong and the ferroelectric state is the ground state. For higher defect concentration, the local polarizations overwhelm forcing a relaxor ground state. This scenario allows the system to exhibit mixed ferroelectric and relaxor states over an extended composition region [63–65]. The abrupt ferroelectric to relaxor cross over at $x > 0.58$ in $(1-x)$KBT-xNBT presents a sharp contrast to the commonly observed gradual evolution. This qualitative difference lies in the nature of the random fields. Here, instead of a localized defect confined to a lattice site, the random field causing disruptions to the long-range ferroelectric order is associated with a ferroelectric incompatible in-phase octahedral tilt, which has correlation length spanning several unit cells (as evident from the fact that they are able diffract the incident neutron beam and show weak superlattice reflections in the neutron powder diffraction patterns). This mesoscopic size random field must be associated with a composition driven ferroelastic instability. Our NPD study suggests that the critical composition for this instability to set in is $x > 0.58$. This explains the abrupt crossover from a normal ferroelectric to a full-blown relaxor state for $x > 0.58$.

The next question is whether the in-phase tilt distortion is coupled to the ferroelectric distortion or not. High temperature NPD studies of the MPB compositions of NBT-BT [48] and NBT-KBT [44,66] have shown that the superlattice peaks corresponding to the in-phase tilt survives even after the ferroelectric order disappears. This suggests that the in-phase tilt, which is the primary source of random field in our system, is not coupled to the ferroelectric order. Rather, this instability sets in in the ergodic temperature regime for $x > 0.58$. The abrupt decrease in the Burn's temperature for $x > 0.58$ suggests that the presence of the in-phase tilt causes difficulty in the formation of the PNRs and requires more cooling vis-à-vis the compositions ($x < 0.60$) that do not show the in-phase tilt. Further, the continuity of this tilt at low temperatures obstructs the development of a long-range ferroelectric order and stabilizes the relaxor ground state. In the absence of this tilt (for $x < 0.60$) the system could acquire a ferroelectric ground state.

We may emphasize that the superlattice peaks corresponding to the in-phase tilt cannot be indexed precisely on a doubled pseudocubic cell. This seems to suggest that the in-phase tilt is not highly ordered to form a long-range $P4bm$ phase as in the high temperature phase (say $> 300\,^{\circ}$C) of NBT. Alternatively, the tilt might be incommensurately modulated, which cannot be explained within the framework of simple octahedral tilt system of Glazer [67]. Diffuse scattering studies of the classical Pb-based relaxors like $Pb(Mg_{1/3}Nb_{2/3})O_3$ (PMN) and $Pb(Zn_{1/3}Nb_{2/3})O_3$ (PZN) have confirmed that the relaxor state is comprised of local atomic displacements associated with the freezing of phonon mode corresponding to the M-point ($k = 1/2, 1/2, 0$) of the cubic Brillouin zone [12,68,69]. The relaxor behavior is strongly coupled to such a nonferroelectric component of the atomic displacement pattern. The visibility of the superlattice peaks corresponding to the M-point distortion in the NPD patterns of our specimens for $x > 0.58$ suggests that this distortion has relatively larger correlation length as compared to that in the classical relaxors. At the same time, the correlation length is not sufficiently large to qualify this distortion as a $P4bm$ phase. Our results suggest that the intermediate scale order in the in-phase tilt allows the ferroelectric correlations to develop albeit on a smaller length scale.

Transmission electron microscopy study of KBT-NBT in the vicinity of the critical composition reported here suggests that the in-phase tilt axis is parallel to the nonpolar a/b axis of the average tetragonal phase [66]. This contrasts with the high temperature $P4bm$ phase of NBT for which the tetragonal axis is also the in-phase tilt axis. These compositions show highly complex domain structure comprising of few tens of nanometers thick tetragonal ($P4mm$)-like twin (T1) domains within which lies nanoscale ($\sim$5 nm) T2 domains of least two different rotational variants [35,66]. The T2 domains are associated with in-phase octahedral tilt with tilt axes parallel to the a/b axes of the average $P4mm$ phase. The average symmetry of the assemblages of the in-phase tilted nanodomains has been proposed to be $I4mm$ or $Imm2$. However, as demonstrated in Fig. S14c, the superlattice peaks cannot be accurately modeled with an average structure within the framework of a $2 \times 2 \times 2$ pseudocubic cell, suggesting the plausibility of an incommensuratelike modulation in the octahedral tilt configuration. Further investigation is required to throw light on the details of this complex structural state. From the ferroelectric perspective, such regions and the neighborhoods around them are structural disorder, which manifests as cubiclike phase in the XRPD study. That even after poling, the disorder regions though significantly reduced, still

survive for $x > 0.58$ is consistent with the persistence of the in-phase tilted regions. The noticeable softening of the lattice on approaching $x = 0.60$ [Fig. 3(c)] as revealed in the Raman study, suggests a correlation of the lattice softening with the disordered/incommensurate in-phase tilt distortion. This softening is likely to contribute to the abrupt enhancement of the dielectric and electromechanical properties for $x > 0.58$.

V. CONCLUSIONS

In summary, in contrast to most ferroelectric perovskite solid solution systems wherein the ferroelectric ground state gives way to a relaxor ground state in a gradual manner with increasing concentration of random-field centers, this crossover is shown to occur abruptly at $x > 0.58$ in $(1-x)K_{0.5}Bi_{05}TiO_3$-$(x)Na_{0.5}Bi_{0.5}TiO_3$. The dramatic change in the polar character at this composition manifests as anomalous change in several physical properties (dielectric, electromechanical, and ferroelectric properties, Burn's temperature) and mimics a scenario often reported for MPB ferroelectric solid solutions. In the present case it is rather associated with an abrupt increase in the structural disorder while the system still retains an average tetragonal ferroelectric distortion on the global scale. We show that this disorder is caused by the onset of a ferroelastic distortion comprised of disordered/incommensuratelike in-phase octahedral tilt in the paraelectric/ergodic relaxor state and its persistence at low temperatures. Our study widens the understanding of the fundamental factors that induce a relaxor state in ferroelectric perovskites, and its direct bearing on the physical properties.

ACKNOWLEDGMENTS

R.R. gratefully acknowledges the Science and Engineering Research Board (SERB) of the Ministry of Science and Technology, Government of India (Grant No. EMR/2016/001457) and Space Technology Cell, IISc (Grant No. STC-0406) for financial assistance. R.R. is grateful to the Alexander von Humboldt foundation for the fellowship to stay in Germany and conduct the neutron powder diffraction studies.

[1] F. Li, D. Lin, Z. Chen, Z. Cheng, J. Wang, C. Li, Z. Xu, Q. Huang, X. Liao, L.-Q. Chen, T. R. Shrout, and S. Zhang, Nat. Mater. **17**, 349 (2018).
[2] X. Liu and X. Tan, Adv. Mater. **28**, 574 (2016).
[3] B. Narayan, J. S. Malhotra, R. Pandey, K. Yaddanapudi, P. Nukala, B. Dkhil, A. Senyshyn, and R. Ranjan, Nat. Mater. **17**, 427 (2018).
[4] R. Pandey, B. Narayan, D. K. Khatua, S. Tyagi, A. Mostaed, M. Abebe, V. Sathe, I. M. Reaney, and R. Ranjan, Phys. Rev. B **97**, 224109 (2018).
[5] P. Li, J. W. Zhai, B. Shen, S. J. Zhang, X. L. Li, F. Y. Zhu, and X. M. Zhang, Adv. Mater. **30**, 1705171 (2018).
[6] F. Li, S. J. Zhang, D. Damjanovic, L. Q. Chen, and T. R. Shrout, Adv. Funct. Mater. **28**, 1801504 (2018).
[7] F. Li, S. Zhang, T. Yang, Z. Xu, N. Zhang, G. Liu, J. Wang, J. Wang, Z. Cheng, Z. G. Ye, J. Luo, T. R. Shrout, and L. Q. Chen, Nat. Commun. **7**, 13807 (2016).
[8] D. Phelan, C. Stock, J. A. Rodriguez-Rivera, S. Chi, J. Leao, X. Long, Y. Xie, A. A. Bokov, Z.-G. Ye, P. Ganesh, and P. M. Gehring, Proc. Nat. Acad. Sci. USA **111**, 1754 (2014).
[9] Z. Kutnjak, J. Petzelt, and R. Blinc, Nature (London) **441**, 956 (2006).
[10] G. Xu, J. Wen, C. Stock, and P. M. Gehring, Nat. Mat. **7**, 562 (2008).
[11] V. M. Ishchuk, V. N. Baumer, and V. L. Sobolev, J. Phys. Condens. Matter **17**, L177 (2005).
[12] N. Takesue, Y. Fujii, M. Ichihara, and H. Chen, Phys. Rev. Lett. **82**, 3709 (1999).
[13] A. R. Akbarzadeh, S. Prosandeev, E. J. Walter, A. Al-Barakaty, and L. Bellaiche, Phys. Rev. Lett. **108**, 257601 (2012).
[14] V. Westphal, W. Kleemann, and M. D. Glinchuk, Phys. Rev. Lett. **68**, 847 (1992).
[15] Y. Yan, S. J. Pennycook, Z. Xu, and D. Viehland, Appl. Phys. Lett. **72**, 3145 (1998).
[16] P. K. Davies and M. A. Akbas, J. Phys. Chem. Solids **61**, 159 (2000).
[17] N. Setter and L. E. Cross, J. Mater. Sci. **15**, 2478 (1980).
[18] N. Setter and L. E. Cross, J. Appl. Phys. **51**, 4356 (1980).
[19] R. Guo, L. E. Cross, S.-E. Park, B. Noheda, D. E. Cox, and G. Shirane, Phys. Rev. Lett. **84**, 5423 (2000).
[20] K. Datta, D. Walker, and P. A. Thomas, Phys. Rev. B **82**, 144108 (2010).
[21] K.V. Lalitha, A. N. Fitch, and R. Ranjan, Phys. Rev. B **87**, 064106 (2013).
[22] R. E. Eitel, C. A. Randall, T. R. Shrout, P. W. Rehrig, W. Hackenberger, and S-E Park, Jpn. J. Appl. Phys. **40**, 5999 (2001).
[23] K. Lin, Z.Y. Zhou, L. Liu, H. Q. Ma, J. Chen, J. X. Deng, J. L. Sun, L. You, H. Kasai, K. Kato, M. Takata, and X. R. Xing, J. Am. Chem. Soc. **137**, 13468 (2015).
[24] Z. Xu, X. H. Dai, J. F. Li, and D. Viehland, Appl. Phys. Lett. **68**, 1628 (1996).
[25] T. Ikeda, T. Haraguchi, Y. Onodera, and T. Saito, Jpn. J. Appl. Phys. **10**, 987 (1971).
[26] X. H. Zheng and X. M. Chen, J. Mater. Res. **17**, 1664 (2002).
[27] X. H. Zheng and X. M. Chen, Solid State Commun. **125**, 449 (2003).
[28] I. Levin, M. C. Stennett, G. C. Miles, D. I. Woodward, A. R. West, and I. M. Reaney, Appl. Phys. Lett. **89**, 122908 (2006).
[29] M. C. Stennett, I. M. Reaney, G. C. Miles, A. R. West, C. A. Kirk, and I. Levin, J. Appl. Phys. **101**, 104114 (2007).
[30] X. Zhu, M. Fu, M. C. Stennett, P. M. Vilarinho, I. Levin, C. A. Randall, J. Gardner, F. D. Morrison, and I. M. Reaney, Chem. Mater. **27**, 3250 (2015).
[31] B. Jiang, T. Grande, and M. Selbach, Chem. Mater. **29**, 4244 (2017).
[32] B. Jiang, T.M. Raeder, D.-Y. Lin, T. Grande, and S. M. Selbach, Chem. Mater. **30**, 2631 (2018).
[33] I. Levin, D. S. Keeble, G. Cibin, H. Y. Playford, M. Eremenko, V. Krayzman, W. J. Laws, and I. M. Reaney, Chem. Mater. **31**, 2450 (2019).

[34] M. Otonicar, S. D. Škapin, B. Jan ˇ car, R. Ubic, and D. Suvorov, J. Am. Ceram. Soc. **93**, 4168 (2010).
[35] M. Otonicar, S. D. Škapin, and B. Jancar, IEEE Trans. Ultrason. Ferroelectr. Freq. Control **58**, 1928 (2011).
[36] M. Hagiwara and S. Fujihara, Appl. Phys. Lett. **107**, 012903 (2015).
[37] M. Hagiwara and S. Fujihara, Jpn. J. Appl. Phys. **54**, 10ND10 (2015).
[38] M. Hagiwara, Y. Ehara, N. Novak, N. H. Khansur, A. Ayrikyan, K. G. Webber, and S. Fujihara, Phys. Rev. B **96**, 014103 (2017).
[39] E. Aksel, J. S. Forrester, J. L. Jones, P. A. Thomas, K. Page, and M. R. Suchomel, Appl. Phys. Lett. **98**, 152901 (2011).
[40] S. Gorfman and P.A. Thomas, J. Appl. Crystallogr. **43**, 1409 (2010).
[41] T. Takenaka, H. Nagata, and Y. Hiruma, IEEE Trans. Ultrason. Ferroelectrc. Freq. Control **56**, 1595 (2009).
[42] G. D. Adhikary, D. K. Khatua, A. Senyshyn, and R. Ranjan, Phys. Rev. B **99**, 174112 (2019).
[43] A. Sasaki, T. Chiba, Y. Mamiya1, and E. Otsuki, Jpn. J. Appl. Phys. **38**, 5564 (1999).
[44] G. D. Adhikary, D. K. Khatua, A. Senyshyn, and R. Ranjan, Acta Mater. **164**, 749 (2019).
[45] M. Hoelzel, A. Senyshyn, R. Gilles, H. Boysen, and H. Fuess, Neutron News **18**, 23 (2007).
[46] J. Rodrigues-Carvajal, *2000 FULLPROF. A Rietveld Refinement and Pattern Matching Analysis Program* (Laboratoire Leon Brillouin (CEACNRS), France).
[47] See Supplemental Material at http://link.aps.org/supplemental/10.1103/PhysRevB.102.184113 for information on pyroelectric and dielectric measurements and Rietveld analysis of NPD and XRPD patterns.
[48] G. D. Adhikary, D. K. Khatua, A. Mishra, A. De, N. Kumar, S. Saha, U. Shankar, A. Senyshyn, B. N. Rao, and R. Ranjan, Phys. Rev. B **100**, 134111 (2019).
[49] Y. Hiruma, R. Aoyagi, H. Nagata, and T. Takenaka, Jpn. J. Appl. Phys. **44**, 5040 (2005).
[50] B. N. Rao, A. N. Fitch, and R. Ranjan, Phys. Rev. B **87**, 060102(R) (2013).
[51] B. N. Rao and R. Ranjan, Phys. Rev. B **86**, 134103 (2012).
[52] J. E. Daniels, W. Jo, J. Rödel, and J. L. Jones, Appl. Phys. Lett. **95**, 0329042009.
[53] N. Khansur, R. Benton, T. Dinh, J. Lee, J. Jones, and J. Daniels, J. Appl. Phys. **119**, 234101 (2016).
[54] U. Shankar, N. Kumar, B. Narayan, D. Swain, A. Senyshyn, and R. Ranjan, Phys. Rev. B **100**, 094101 (2019).
[55] T. Steilmann, B. J. Maier, M. Gospodinov, U. Bismayer, and B. Mihailova, J. Phys.: Condens. Matter **26**, 175401 (2014).
[56] J. Kreisel, A. M. Glazer, G. Jones, P. A. Thomas, L. Abello, and G. Lucazeau, J. Phys.: Condens. Matter **12**, 3267 (2000).
[57] J. Kreisel, A. M. Glazer, P. Bouvier, and G. Lucazeau, Phys. Rev. B **63**, 174106 (2001).
[58] M. K. Niranjan, T. Karthik, S. Asthana, J. Pan, and U. V. Waghmare, J. Appl. Phys. **113**, 194106 (2013).
[59] S. Prosandeev, D. Wang, W. Ren, J. Iniguez, and L. Bellaiche, Adv. Funct. Mater. **23**, 234 (2013).
[60] R. Garg, B. N. Rao, A. Senyshyn, and R. Ranjan, J. Appl. Phys. **114**, 234102 (2013).
[61] D. K. Khatua, A. Senyshyn, and R. Ranjan, Phys. Rev. B **93**, 134106 (2016).
[62] D. Wang, X. Ke, Y. Wang, J. Gao, Y. Wang, L. Zhang, S. Yang, and X. Ren, Phys. Rev. B **86**, 054120 (2012)].
[63] Y. Liu, R. L. Withers, B. Nguyen, and K. Elliott, Appl. Phys. Lett. **91**, 152907 (2007).
[64] V. V. Shvartsman, J. Dec, Z. K. Xu, J. Banys, P. Keburis, and W. Kleemann, Phase Trans. **81**, 1013 (2008).
[65] C. Lei, A. A. Bokov, and Z.-G. Ye, J. Appl. Phys. **101**, 084105 (2007).
[66] I. Levin, I. M. Reaney, E.-M. Anton, W. Jo, J. Rödel, J. Pokorny, L. A. Schmitt, H.-J. Kleebe, M. Hinterstein, and J. L. Jones, Phys. Rev. B **87**, 024113 (2013).
[67] A. M. Glazer, Acta Crystallogr. Sec. A **31**, 756 (1975).
[68] G. Xu, P. M. Gehring, and G. Shirane, Phys. Rev. B **74**, 104110 (2006).
[69] S. B. Vakhrushev, A. A. Naberezhnov, N. M. Okuneva, and B. N. Savenko, Sov. Phys. Solid State **37**, 1993 (1995).